

RESEARCH ARTICLE

View Article Online  
View Journal | View Issue



Cite this: *Mater. Chem. Front.*,  
2020, 4, 3226

# Physicochemical surface-structure studies of highly active zirconocene polymerisation catalysts on solid polymethylaluminoxane activating supports†

Alexander F. R. Kilpatrick, , Nicholas H. Rees, , Zoë R. Turner,   
Jean-Charles Buffet and Dermot O'Hare \*

Physicochemical surface-structure studies of highly active slurry-phase ethylene polymerisation catalysts has been performed. Zirconocene complexes immobilised on solid polymethylaluminoxane (sMAO) (sMAO-Cp<sub>2</sub>ZrX<sub>2</sub>), have been investigated using SEM-EDX, diffuse reflectance FT-IR (DRIFT) and high field (21.1 T) solid state NMR (ssNMR) spectroscopy. The data suggest a common surface-bound cationic methylzirconocene is the catalytically active species. <sup>91</sup>Zr solid state NMR spectra of sMAO-Cp<sub>2</sub>ZrCl<sub>2</sub> and sMAO-Cp<sub>2</sub>ZrMe<sub>2</sub> are consistent with a common surface-bound Zr environment. However, variation of the σ-donor (X) groups on the metallocene precatalyst leads to significant differences in polymerisation activity. We report evidence for X group transfer from the precatalyst complex onto the surface of the aluminoxane support, which in the case of X = C<sub>6</sub>F<sub>5</sub>, results in a 38% increase in activity.

Received 14th July 2020,  
Accepted 7th September 2020

DOI: 10.1039/d0qm00482k

rsc.li/frontiers-materials

## Introduction

Methylaluminoxane (MAO) is the most commonly used activator and co-catalyst for transition metal containing, single-site complexes in olefin polymerisation.<sup>1,2</sup> The combination of MAO, an inert inorganic carrier material (most commonly silica) and a precatalyst complex have been described by Severn as the “Holy Trinity” of supported single-site catalysts.<sup>3</sup> However, there is also growing interest in single-site catalysts in particle forming polymerisation processes that are free from an inert inorganic carrier.<sup>4</sup> These require an activating support material, which can be combined with the precatalyst complex in a single synthetic step.<sup>5–9</sup> This process has several advantages from an industrial viewpoint, as it reduces the time and energy-intensive drying steps and hence can lower manufacturing costs. Furthermore, these ‘self-supported’ catalyst systems have an advantage over silica-supported systems as the complex loading can be increased significantly, which leads to correspondingly higher polymerisation activities.

In 2013, Tosoh Finechem Corporation reported, in the patent literature, an insoluble form of solid methylaluminoxane (sMAO) formed *via* controlled hydrolysis of trimethylaluminium with

benzoic acid.<sup>10</sup> We have recently reported the laboratory scale synthesis and detailed characterisation of sMAO,<sup>11</sup> and demonstrated its function as a solid-phase support, scavenger and activator in slurry-phase ethylene polymerisation.<sup>12–14</sup> Observed activities are significantly higher than for other supports; for example sMAO-*rac*-ethylenebis(1-permethylindeyl)zirconium dichloride is at least three times more active than its silica-supported MAO counterpart (5365 vs. 1649 kg<sub>PE</sub> mol<sub>Zr</sub><sup>−1</sup> h<sup>−1</sup> bar<sup>−1</sup> respectively).<sup>15,16</sup>

Furthermore, we have shown that reaction of sMAO with tris(pentafluorophenyl)borane or pentafluorophenol produces highly active modified-sMAO supports which show enhanced polymerisation activity with both *rac*-ethylenebis(1-indenyl) zirconium dichloride, *rac*-(EBI)ZrCl<sub>2</sub>,<sup>17</sup> and a range of unsymmetrical *ansa*-bridged permethylindenyl complexes.<sup>18</sup>

Characterisation of sMAO using multinuclear NMR spectroscopy in solution and in the solid state reveals an aluminoxane structure that features “structural” and “free” AlMe<sub>x</sub> units in addition to benzoate residues. Total X-ray scattering measurements on sMAO allow comparisons to be made with simulated data from DFT modelled structures of MAO. Of these, the best fit to the experimental X-ray scattering data resulted from TMA-capped nanotubular and spherical cage structures, (AlOMe)<sub>9</sub>·(AlMe<sub>3</sub>)<sub>3</sub> and (AlOMe)<sub>20</sub>·(AlMe<sub>3</sub>)<sub>n</sub>, *n* = 1, 2, respectively.<sup>19,20</sup>

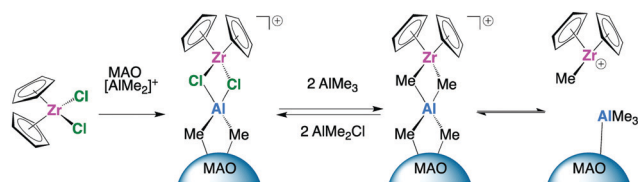
Our current efforts are focussed on elucidating the structure and chemical environment of the active polymerising species in sMAO supported catalysts. Significant progress has been made in the last few years to determine the function of MAO as a

Chemistry Research Laboratory, Department of Chemistry, University of Oxford,

12 Mansfield Road, Oxford, OX1 3TA, UK. E-mail: dermot.ohare@chem.ox.ac.uk

† Electronic supplementary information (ESI) available: Experimental details (general procedures, syntheses and ethylene polymerisation), additional characterising data (solution and solid state NMR spectroscopy, DRIFTS, SEM-EDX analysis), SEM images for polyethylene samples. See DOI: 10.1039/d0qm00482k





**Scheme 1** Simplified mechanism for metallocene activation by  $[AlMe_2]^+$  groups in silica-MAO, proposed by Weckhuysen and co-workers.<sup>32,33</sup>

source of the electrophilic cation  $[AlMe_2]^+$ , which plays a key role in the activation of metallocene complexes in solution.<sup>21–31</sup>

Weckhuysen and co-workers have recently proposed a similar mechanism which operates in the genesis of the active site for  $\{1,3\text{-}n\text{Bu},\text{Me}\}\text{Cp}_2\text{ZrCl}_2$  immobilised on silica-MAO (Scheme 1).<sup>32,33</sup> Specifically, metallocene activation occurs by the complexation of the precursor with weak Lewis acid sites of silica-MAO, which are a source of mobile  $[AlMe_2]^+$  groups, leading to formation of the active cationic zirconocene species stabilised on the surface by MAO.

This has prompted us to investigate in more detail the nature of the active species generated in sMAO supported zirconocene systems. We have chosen a series of zirconocene(IV) precatalyst complexes due to the relative simplicity of their ligand environments which allows more facile characterisation, and enables comparison with previous studies of the active species in homogeneous and heterogeneous single-site catalyst systems.<sup>34–37</sup>

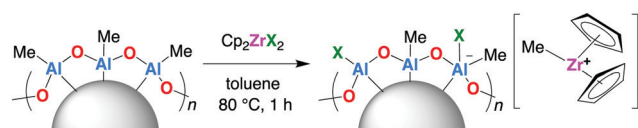
We have employed a combination of characterisation methods, including high field solid state nuclear magnetic resonance (ssNMR) spectroscopy, SEM-EDX elemental mapping and diffuse-reflectance FT-IR spectroscopy. Through these fundamental investigations into the active species, we aim to establish structure/catalytic activity relationships for the immobilised complex and solid support.

## Results and discussion

### Catalyst synthesis and characterisation

A series of zirconocene(IV) complexes,  $\text{Cp}_2\text{ZrX}_2$  ( $X = \text{Cl}, \text{Me}, \text{Br}, \text{Ph}, \text{C}_6\text{F}_5, \text{OC}_6\text{F}_5$ ),  $n\text{BuCp}_2\text{ZrCl}_2$ ,  $\text{rac}(\text{EBI})\text{ZrCl}_2$ ,  $\text{Me}_2\text{Si}(\text{C}_5\text{H}_4)_2\text{ZrCl}_2$  and  $\text{Me}_2\text{Si}(\text{C}_5\text{H}_4)_2\text{ZrMe}_2$  were selected as precatalysts for this study. In each case, the supported complex-sMAO sample was synthesised by addition of toluene to a mixture of solid support and complex (initial loading  $[Al_{\text{sMAO}}]_0/[Zr]_0$  of 50), followed by heating at 80 °C for 1 h. After workup, bright orange powders were isolated in > 85% yield (Scheme 2).

Elemental analysis of these catalysts using ICP-MS is presented in Table 1. The aluminium content of the final catalysts remains approximately constant across the series, slightly reduced from



**Scheme 2** Synthesis of a generic sMAO- $\text{Cp}_2\text{ZrX}_2$  catalyst and schematic representation of its proposed structure.

**Table 1** Elemental analysis and ethylene polymerisation data for supported complex-sMAO catalysts at target loading  $[Al_{\text{sMAO}}]_0/[Zr]_0 = 50$

Complex	Al (wt%)	Zr (wt%)	$[Al_{\text{sMAO}}]_0/[Zr]_0$
$\text{Cp}_2\text{ZrCl}_2$	36.2	2.36	51.7
$\text{Cp}_2\text{ZrMe}_2$	37.0	2.32	53.9
$\text{Cp}_2\text{ZrBr}_2$	34.1	1.71	67.4
$\text{Cp}_2\text{Zr}(\text{C}_6\text{H}_5)_2$	34.2	1.78	65.1
$\text{Cp}_2\text{Zr}(\text{C}_6\text{F}_5)_2$	35.1	1.73	68.6
$\text{Cp}_2\text{Zr}(\text{OC}_6\text{F}_5)_2$	34.4	1.69	68.8
$n\text{BuCp}_2\text{ZrCl}_2$	36.2	2.26	54.3
$\text{rac}(\text{EBI})\text{ZrCl}_2$	34.9	2.26	52.1
$\text{Me}_2\text{Si}(\text{C}_5\text{H}_4)_2\text{ZrCl}_2$	35.7	2.08	58.1
$\text{Me}_2\text{Si}(\text{C}_5\text{H}_4)_2\text{ZrMe}_2$	37.6	2.40	53.1

Immobilisation conditions: sMAO-complex ( $[Al_{\text{sMAO}}]_0/[Zr]_0 = 50$ ), 80 °C, 60 minutes, toluene (30 mL). All elemental analysis experiments were conducted three times to ensure the reproducibility of the corresponding outcome.

that of the sMAO support (40.2 wt%Al). For all sMAO- $\text{Cp}^R\text{ZrCl}_2$  catalysts, the  $[Al_{\text{sMAO}}]_0/[Zr]_0$  molar ratio determined was close to the targeted ratio of 50, consistent with full complex immobilisation. This confirms that the degree of immobilisation of zirconocene dichloride complexes is not affected by the different ancillary  $\text{Cp}^R$  ligands. This can be attributed to the high surface area (*ca.* 600 m<sup>2</sup> g<sup>−1</sup>) and reactivity of sMAO in which all surface sites can activate zirconocene complexes. The high concentration of active “Al-Me” moieties is beneficial when compared to MAO-impregnated silica supports, which generally show a lower surface area (*ca.* 275 m<sup>2</sup> g<sup>−1</sup>) and hence  $[Al_{\text{sMAO}}]_0/[Zr]_0$  loadings below 131 cannot be achieved without complex leaching and significant reactor fouling. Furthermore, inert carrier supports possess -OH groups which provide a pathway for complex deactivation.<sup>32,38</sup> Comparison of the  $[Al_{\text{sMAO}}]_0/[Zr]_0$  data for chloride and methide complexes with the same  $\text{Cp}^R$  ligands,  $\text{Cp}_2\text{ZrX}_2$  and  $\text{Me}_2\text{Si}(\text{C}_5\text{H}_4)_2\text{ZrX}_2$  ( $X = \text{Cl}, \text{Me}$ ), reveals that both chloride and methide leaving groups result in near-quantitative complex immobilisation. However, the sMAO- $\text{Cp}_2\text{ZrX}_2$  catalysts derived from metallocenes with aryl and aryloxy  $\sigma$ -donor groups ( $X = \text{Ph}, \text{C}_6\text{F}_5, \text{OC}_6\text{F}_5$ ) show slightly higher  $[Al_{\text{sMAO}}]_0/[Zr]_0$  values, suggesting the larger leaving group limits the extent of complex immobilisation under these conditions.

Solid MAO is insoluble in aromatic and aliphatic hydrocarbons but is sufficiently soluble in THF-*d*<sub>8</sub>, to be studied by solution NMR spectroscopy. However, efforts to apply solution NMR spectroscopy to characterise sMAO-complex samples was complicated by leaching of the zirconocene upon addition of THF-*d*<sub>8</sub>.

Solid-state NMR spectroscopy has been increasingly applied for characterisation of supported organometallic complexes,<sup>39–41</sup> and has proved a powerful tool for the structural elucidation of immobilised single-site zirconocene catalysts.<sup>34,35,42,43</sup> For these experiments samples of sMAO- $\text{Cp}_2\text{ZrX}_2$  ( $X = \text{Cl}, \text{Me}$ ) with  $[Al_{\text{sMAO}}]_0/[Zr]_0 = 25$  were prepared according to Scheme 2, which produced brightly coloured solids that settled beneath a colourless supernatant solution. Elemental analysis by ICP-MS provided a zirconium content of 3.22 and 4.16 wt% for sMAO- $\text{Cp}_2\text{ZrCl}_2$  and sMAO- $\text{Cp}_2\text{ZrMe}_2$  respectively.



Samples of sMAO-Cp<sub>2</sub>ZrCl<sub>2</sub> and sMAO-Cp<sub>2</sub>ZrMe<sub>2</sub> show identical <sup>1</sup>H DEPTH ssNMR spectra (Fig. S6 and S8, ESI†)<sup>44</sup> with resonances at δ<sub>H</sub> −0.4 and 6.8 ppm assigned to Al-CH<sub>3</sub> and Zr-CpH environments of the sMAO support and immobilised zirconocene species, respectively. <sup>13</sup>C CP-MAS spectra of sMAO-Cp<sub>2</sub>ZrCl<sub>2</sub> and sMAO-Cp<sub>2</sub>ZrMe<sub>2</sub> (Fig. S5 and S7, ESI†) both show signals at −7 and 177 ppm, assigned to the Al-methyl and benzoate groups in sMAO, and resonances at 114 and 128 ppm assigned to Zr-Cp environments. A broad resonance is observed at 50 ppm, in the expected region for a Zr-CH<sub>3</sub> group,<sup>42</sup> however, the low intensity means we cannot be unequivocal in this assignment. An analogous sample synthesised with Cp<sub>2</sub>Zr(<sup>13</sup>CH<sub>3</sub>)<sub>2</sub> (Fig. 1) shows significant signal enhancement in the <sup>13</sup>C CP-MAS spectrum at −7 ppm and a relatively low signal enhancement at 50 ppm, suggesting the labelled methyl groups are scrambled with the Al-Me groups of the sMAO support.

Solid state <sup>91</sup>Zr NMR is a logical choice for the characterisation of immobilised metallocene catalysts. However, <sup>91</sup>Zr ssNMR studies of organometallic zirconium complexes are rare owing to the relatively low sensitivity of <sup>91</sup>Zr (*I* = 5/2), due to a low natural abundance (11.23%) and a relatively low gyromagnetic ratio (−2.49750 × 10<sup>7</sup> rad T<sup>−1</sup> s<sup>−1</sup>). Despite these challenges, Schurko and co-workers have reported in-depth <sup>91</sup>Zr ssNMR studies of a range of zirconocenes,<sup>45,46</sup> including olefin polymerisation precatalysts Cp<sub>2</sub>ZrCl<sub>2</sub> and Cp<sub>2</sub>ZrMe<sub>2</sub>. However, no follow-up studies for <sup>91</sup>Zr ssNMR characterisation of heterogeneous catalyst systems have been published, presumably owing to the low wt% Zr in supported complexes that are also active for polymerisation.

The Quadrupolar Carr Purcell Meiboom Gill (QCPMG) technique is a common method used to measure broad NMR signals from quadrupolar nuclei.<sup>47–49</sup> The static QCPMG subspectra of sMAO-Cp<sub>2</sub>ZrX<sub>2</sub> (X = Cl, Me) samples in a 7 mm o.d. silicon nitride rotor were acquired in a piecewise fashion using 51 420 Hz irradiation frequency offsets (integer multiple of 1/τ<sub>a</sub>) until no further signal could be detected upon further increase or decrease of the transmitter frequency. The QCPMG experiment

gives spectra in the form of a manifold of spikelets which are offset from the irradiation frequency by 1/τ<sub>a</sub>; therefore, differentiation of nonequivalent sites by chemical shift is not possible unless gross differences (*i.e.*, fairly distinct overlapping powder patterns) can be observed. The co-added spectra for pure Cp<sub>2</sub>ZrCl<sub>2</sub> and Cp<sub>2</sub>ZrMe<sub>2</sub> (Fig. 2a and b, respectively) show significant differences to each other, the latter complex showing a broader spikelet pattern consistent with a larger quadrupolar coupling constant (*C*<sub>Q</sub>).<sup>45,46</sup> Spectra for immobilised complexes sMAO-Cp<sub>2</sub>ZrCl<sub>2</sub> and sMAO-Cp<sub>2</sub>ZrMe<sub>2</sub> (Fig. 2c and d, respectively) show complex spikelet patterns that are qualitatively similar, with breadths of 196 and 194 kHz respectively. Unfortunately, the chemical shift dispersion at *B*<sub>0</sub> of 21.1 T is insufficient to resolve if any non-equivalent Zr sites are present. Nonetheless, the clear similarities in the <sup>91</sup>Zr ssNMR spectra of sMAO-Cp<sub>2</sub>ZrCl<sub>2</sub> and sMAO-Cp<sub>2</sub>ZrMe<sub>2</sub> are consistent with common surface-bound Zr environments, and provide a useful “fingerprint” for the supported complexes.

Diffuse reflectance Fourier transform infrared (DRIFT) spectroscopy was employed to further characterise the supported catalysts. The DRIFT spectra of sMAO-Cp<sub>2</sub>ZrCl<sub>2</sub> and sMAO-Cp<sub>2</sub>ZrMe<sub>2</sub> ([Al]<sub>sMAO</sub>/[Zr]<sub>0</sub> = 25) both show strong IR bands at *ca.* 840 cm<sup>−1</sup> in addition to those of the sMAO support (Fig. S23, ESI†).<sup>17</sup> An in-depth IR study of MAO-metalocene reaction mixtures by Eilertsen *et al.* attributed IR bands around 820 cm<sup>−1</sup> to a cationic species containing a methyl bridge between Zr and Al, that is active for ethylene polymerisation.<sup>50</sup> This provides supporting evidence for methylation of the Zr-Cl bond on immobilisation of Cp<sub>2</sub>ZrCl<sub>2</sub> with sMAO.

The spatial distribution of Al, O, Zr and Cl on the surface of the immobilised catalysts was investigated by Scanning Electron Microscopy (SEM) together with Energy Dispersive X-ray (EDX) spectroscopy. An [Al]<sub>sMAO</sub>/[Zr]<sub>0</sub> = 25 was required in order to observe the immobilised zirconium species (<5 wt% Zr) by EDX spectroscopy. Elemental mapping of sMAO-Cp<sub>2</sub>ZrCl<sub>2</sub> (Fig. 3) reveals a homogeneous distribution of Zr and Cl on the sMAO particles, and sMAO-Cp<sub>2</sub>ZrMe<sub>2</sub> shows a similar distribution of Zr with no Cl detected. These data are consistent with a “single-site” Zr species that forms with concomitant transfer of a σ-donor group, X<sup>−</sup>, onto an Al site on the sMAO support. In the case of sMAO-Cp<sub>2</sub>ZrCl<sub>2</sub>, homogeneous chlorination of the support could occur *via* direct Cl<sup>−</sup> abstraction from the metallocene dichloride precursor by strong Lewis acid sites in the solid activator.<sup>32,33</sup> Alternatively, based on a [AlMe<sub>2</sub>]<sup>+</sup>-assisted activation mechanism, sMAO chlorination could occur *via* net exchange of surface AlMe<sub>3</sub> sites for AlMe<sub>2</sub>Cl, which is formed as a byproduct of catalyst methylation (Scheme 1).<sup>51</sup>

### Slurry-phase ethylene polymerisation studies

The series of sMAO-complex ([Al]<sub>sMAO</sub>/[Zr]<sub>0</sub> = 50) catalysts were tested for slurry-phase ethylene polymerisation capability.

Comparing the activity data (Table 2) for supported zirconocene dichloride catalysts with different Cp<sup>R</sup> ligands reveals a wide range in activity values, with *rac*-(EBI)ZrCl<sub>2</sub> and Me<sub>2</sub>Si(C<sub>5</sub>H<sub>4</sub>)<sub>2</sub>ZrCl<sub>2</sub> displaying the highest and lowest activities,

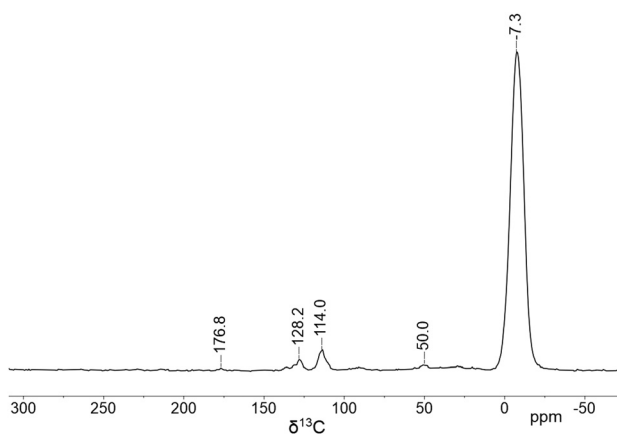


Fig. 1 <sup>1</sup>H → <sup>13</sup>C CP-MAS ssNMR spectrum (10 kHz spinning) of sMAO-Cp<sub>2</sub>Zr(<sup>13</sup>CH<sub>3</sub>)<sub>2</sub>.



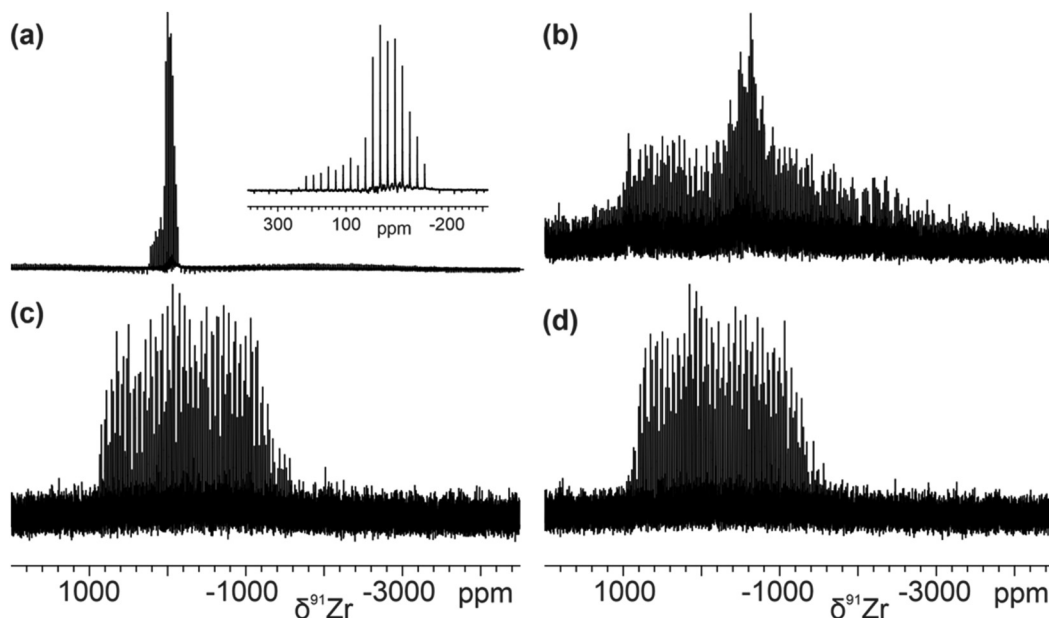


Fig. 2 Static  $^{91}\text{Zr}$  ssNMR spectra of (a)  $\text{Cp}_2\text{ZrCl}_2$  (zoom inset), (b)  $\text{Cp}_2\text{ZrMe}_2$ , (c)  $\text{sMAO-Cp}_2\text{ZrCl}_2$  and (d)  $\text{sMAO-Cp}_2\text{ZrMe}_2$  ( $[\text{Al}_{\text{sMAO}}]_0/[\text{Zr}]_0 = 25$ ) at a field of 21.1 T.

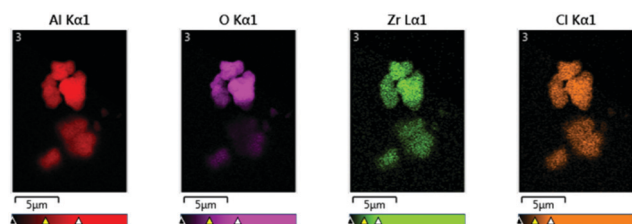


Fig. 3 SEM-EDX analysis of  $\text{sMAO-Cp}_2\text{ZrCl}_2$  ( $[\text{Al}_{\text{sMAO}}]_0/[\text{Zr}]_0 = 25$ ), particles showing elemental mapping for Al (red), O (purple), Cl (orange) and Zr (green).

Table 2 Ethylene polymerisation and molecular weights data for supported complex-sMAO catalysts at target loading  $[\text{Al}_{\text{sMAO}}]_0/[\text{Zr}]_0 = 50$

Complex	Activity/ $10^2$ ( $\text{kg}_{\text{PE}} \text{mol}_{\text{Zr}}^{-1} \text{h}^{-1}$ )	Productivity ( $\text{kg}_{\text{PE}} \text{g}_{\text{cat}}^{-1} \text{h}^{-1}$ )	$M_w$ (kDa)	$M_w/M_n$
$\text{Cp}_2\text{ZrCl}_2$	9.54	0.26	205.9	3.4
$\text{Cp}_2\text{ZrMe}_2$	10.5	0.29	202.6	3.3
$\text{Cp}_2\text{ZrBr}_2$	5.16	0.14	276.9	3.0
$\text{Cp}_2\text{Zr}(\text{C}_6\text{H}_5)_2$	9.78	0.26	232.2	3.2
$\text{Cp}_2\text{Zr}(\text{C}_6\text{F}_5)_2$	11.6	0.30	229.3	3.2
$\text{Cp}_2\text{Zr}(\text{OC}_6\text{F}_5)_2$	9.10	0.23	217.9	3.0
$n\text{BuCp}_2\text{ZrCl}_2$	19.3	0.51	218.0	3.1
$\text{rac}(\text{EBI})\text{ZrCl}_2$	36.4	0.69	88.6	4.0
$\text{Me}_2\text{Si}(\text{C}_5\text{H}_4)_2\text{ZrCl}_2$	2.92	0.079	44.8	3.5
$\text{Me}_2\text{Si}(\text{C}_5\text{H}_4)_2\text{ZrMe}_2$	5.34	0.15	42.2	3.2

Polymerisation conditions: 10 mg catalyst, 2 bar  $\text{C}_2\text{H}_4$ , 70 °C, 30 minutes,  $[\text{Al}_{\text{TIBA}}]_0/[\text{Zr}]_0 = 1000$ , hexanes (50 mL). All polymerisation experiments were conducted at least twice to ensure the reproducibility of the corresponding outcome and mean activity values are quoted correct to 3 significant figures.

respectively ( $3640$  and  $292 \text{ kg}_{\text{PE}} \text{mol}_{\text{Zr}}^{-1} \text{h}^{-1}$ ). Comparing the activity data for  $\text{sMAO-Cp}_2\text{ZrX}_2$  catalysts ( $\text{X} = \text{Cl}, \text{Me}, \text{Br}, \text{Ph}, \text{C}_6\text{F}_5, \text{OC}_6\text{F}_5$ ) reveals a maximum for  $\text{Cp}_2\text{Zr}(\text{C}_6\text{F}_5)_2$  and minimum for  $\text{Cp}_2\text{ZrBr}_2$  ( $1160$  and  $516 \text{ kg}_{\text{PE}} \text{mol}_{\text{Zr}}^{-1} \text{h}^{-1}$  respectively). In general, the  $\text{sMAO}(\text{EBI})\text{ZrCl}_2$  catalyst produces polyethylene with lower molecular weights ( $M_w$  of  $88.6 \text{ kDa}$ ) and slightly broader molecular weight distribution (MWD,  $M_w/M_n$  of  $4.0$ ) than the zirconocene catalyst systems with  $\text{Cp}^R$  ligands ( $210 \text{ kDa} < M_w < 277 \text{ kDa}$ ;  $3.1 < M_w/M_n < 3.4$ ). Despite the high  $[\text{Al}_{\text{sMAO}}]_0/[\text{Zr}]_0$  loadings used in these heterogeneous systems, the absence of reactor fouling and good polymer properties can be attributed to single-site catalytic behaviour.

Differential scanning calorimetry (DSC) analysis of the polyethylenes produced by supported complex-sMAO catalysts based on  $\text{Cp}_2\text{ZrBr}_2$ ,  $\text{Cp}_2\text{Zr}(\text{C}_6\text{F}_5)_2$ ,  $\text{Cp}_2\text{Zr}(\text{OC}_6\text{F}_5)_2$  and  $\text{Me}_2\text{Si}(\text{C}_5\text{H}_4)_2\text{ZrCl}_2$  revealed crystallisation temperatures ( $T_c$ ) between  $116$  and  $117$  °C during the first cooling cycle and melting temperatures ( $T_m$ ) of  $129$ – $135$  °C during the second heating cycle (Fig. 4 and Table S4, ESI<sup>†</sup>), indicative of HDPE with minimal defects and branching.<sup>52,53</sup>

SEM imaging of the polyethylene samples reveals good morphology of the polymer despite the high  $[\text{Al}_{\text{sMAO}}]_0/[\text{Zr}]_0$  loadings used in the catalysts. For the  $\text{sMAO-Cp}_2\text{ZrCl}_2$  system ( $[\text{Al}_{\text{sMAO}}]_0/[\text{Zr}]_0 = 50$ ), smooth popcorn-like polyethylene particles with low levels of aggregation are observed, which mimic the morphology of the catalyst particles (Fig. 5).

These slurry-phase polymerisation data are consistent with longstanding observations for solution phase MAO-zirconocene catalysts, namely that the ancillary  $\text{Cp}^R$  has a primary effect on activity and polymer properties. However, our data show that the change of  $\sigma$ -donor group on the metallocene also has a significant effect on catalyst performance.

In the sMAO supported catalyst system the postulated active species is a charged zirconocene species which is grafted onto





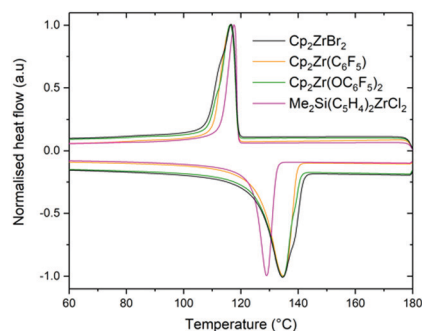
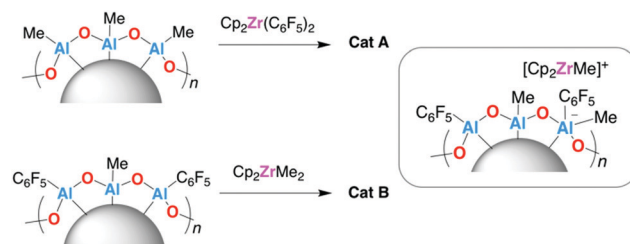


Fig. 4 DSC plot showing the first cooling cycle and second heating cycle for the polyethylenes produced using sMAO-supported  $\text{Cp}_2\text{ZrBr}_2$  (black),  $\text{Cp}_2\text{Zr}(\text{C}_6\text{F}_5)_2$  (orange),  $\text{Cp}_2\text{Zr}(\text{OC}_6\text{F}_5)_2$  (green), and  $\text{Me}_2\text{Si}(\text{C}_5\text{H}_4)_2\text{ZrCl}_2$  (pink). Normalised for clarity.

the aluminosilicate surface primarily by electrostatic interactions (Scheme 2). The steric and electronic demands of the  $\text{Cp}^R$  ligands bound to the zirconocene species are assumed to have a large influence on its relative stability, and hence on the rates of propagation and termination steps in the polymerisation reaction.

We have previously reported that modified sMAO supports, in which surface methyl groups are exchanged for  $\text{C}_6\text{F}_5$  or  $\text{OC}_6\text{F}_5$  groups, result in activity increases with  $\text{rac}(\text{EBI})\text{ZrCl}_2$  compared with to the same catalyst precursor on unmodified sMAO.<sup>17</sup> One possible explanation is that the surface-bound  $\text{C}_6\text{F}_5$  and  $\text{C}_6\text{F}_5\text{O}$  groups on the support lead to an increase in separation between the charged species formed after zirconocene activation, which in turn enhances the performance of the catalytically active species. According to the proposed activation of a  $\text{Cp}_2\text{ZrX}_2$  precatalyst by sMAO (Scheme 2) the  $\sigma$ -donor groups are transferred from zirconium onto the aluminosilicate surface. In effect this produces a modified support which can have a secondary influence on the zirconocene species involved in the polymerisation.

To test this hypothesis, catalyst samples were synthesised from a pentafluorophenyl modified polymethylaluminosilicate support, sMMAO( $\text{C}_6\text{F}_5$ ), and the dimethylzirconocene complex,



Scheme 3 Synthesis of sMAO- $\text{Cp}_2\text{Zr}(\text{C}_6\text{F}_5)_2$  (**Cat A**), sMMAO( $\text{C}_6\text{F}_5$ )- $\text{Cp}_2\text{ZrMe}_2$  (**Cat B**) and a schematic representation of the proposed structure. Immobilisation conditions: sMAO-complex ( $[\text{Al}_{\text{sMAO}}]_0/[\text{Zr}]_0 = 25$ ), 80 °C, 60 minutes, toluene (30 mL).

$\text{Cp}_2\text{ZrMe}_2$  (Scheme 3). The corresponding modifier loading with respect to  $[\text{Al}_{\text{sMAO}}]_0$  was selected to give an approximately equal concentration of  $\text{C}_6\text{F}_5$  groups as the sMAO- $\text{Cp}_2\text{Zr}(\text{C}_6\text{F}_5)_2$  catalyst with target  $[\text{Al}_{\text{sMAO}}]_0/[\text{Zr}]_0$  loading of 25. Catalyst samples sMMAO( $\text{C}_6\text{F}_5$ )- $\text{Cp}_2\text{ZrMe}_2$  (**Cat A**) and sMAO- $\text{Cp}_2\text{Zr}(\text{C}_6\text{F}_5)_2$  (**Cat B**) were characterised by SEM-EDX analysis and solid-state NMR spectroscopy and tested for ethylene polymerisation.

The  $^{19}\text{F}\{^1\text{H}\}$  DEPTH SSNMR spectra of **Cat A** and **Cat B** (Fig. S13 and S22, ESI†) show very similar features, with resonances centred at  $-121$ ,  $-162$  (shoulder) and  $-166$  ppm, assigned to aluminium bound  $\text{C}_6\text{F}_5$  groups. Furthermore, the  $^{19}\text{F}\{^1\text{H}\}$  NMR spectra of both **Cat A** and **Cat B** in  $\text{THF}-d_8$  solution (Fig. S2 and S4, ESI†) consist of three  $^{19}\text{F}$  resonances with identical chemical shift values ( $-123.2$ ,  $-158.3$  and  $-164.2$  ppm). These  $^{19}\text{F}$  NMR spectra are also near identical to those of the  $\text{C}_6\text{F}_5$  modified sMAO supports,<sup>17</sup> consistent with quantitative  $\text{C}_6\text{F}_5$  group transfer from Zr to Al in the immobilisation reaction.

The slurry-phase ethylene polymerisation activity data for **Cat A** and **Cat B** (Table S4, ESI†) are the same within error ( $772$  and  $776 \text{ kg}_{\text{PE}} \text{ mol}_{\text{Zr}}^{-1} \text{ h}^{-1}$  respectively) and 38% higher than that of an unfluorinated control catalyst system sMAO- $\text{Cp}_2\text{ZrMe}_2$  ( $560 \text{ kg}_{\text{PE}} \text{ mol}_{\text{Zr}}^{-1} \text{ h}^{-1}$ ). GPC analysis of the polyethylenes produced by **Cat A** and **Cat B** reveals similar molecular weights ( $M_w$  of  $223.8$  and  $239.5 \text{ kDa}$  respectively) and molecular weight distribution ( $M_w/M_n$  of  $3.1$  and  $3.2$  respectively), consistent with a common active species.

The observed activity enhancement is particular to the  $\text{C}_6\text{F}_5$  complex-support system. Further polymerisation studies with sMAO- $\text{Cp}_2\text{ZrCl}_2$  and sMAO- $\text{Cp}_2\text{ZrMe}_2$  catalysts in a range of  $[\text{Al}_{\text{sMAO}}]_0/[\text{Zr}]_0$  ratios ( $300$ ,  $200$ ,  $100$ ,  $50$  and  $25$ ) show similar activity values at each complex loading (Table S3 and Fig. S26, ESI†). In these cases, the difference between Cl or Me ligand transfer from complex to support does not significantly affect the polymerisation activity.

## Conclusions

Solid methylaluminosilicate, sMAO, has been shown to be an effective activating support for simple zirconocene complexes,  $\text{Cp}^R_2\text{ZrX}_2$ , up to a maximum  $[\text{Al}]_0/[\text{Zr}]_0$  loading of  $25$ . We attribute this to the high surface area ( $\text{ca. } 600 \text{ m}^2 \text{ g}^{-1}$ ) and concentration of highly reactive and accessible “Al–Me” sites.

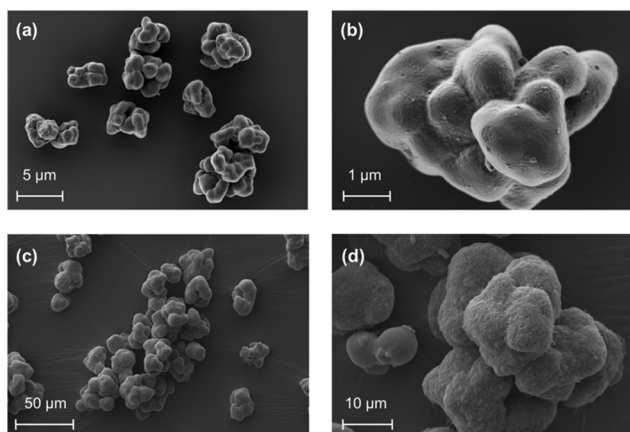


Fig. 5 SEM images of sMAO- $\text{Cp}_2\text{ZrCl}_2$   $[\text{Al}]_0/[\text{Zr}]_0 = 50$  catalyst, at (a)  $\times 3.81\text{k}$ ; (b)  $\times 17.4\text{k}$  magnification, and a polyethylene sample obtained from this catalyst system, at (c)  $\times 500$ ; (d)  $\times 2.0\text{k}$  magnification.



Such a high complex loading enables in-depth characterisation of the final functional catalyst that currently is not possible for zirconocenes with other MAO-impregnated inorganic supports.

$^{13}\text{C}$  CP-MAS ssNMR and DRIFT spectroscopy evidence herein points to a  $[\text{Cp}_2\text{ZrMe}]^+$  species for the sMAO- $\text{Cp}_2\text{ZrMe}_2$  system. Moreover, static  $^{91}\text{Zr}$  ssNMR and DRIFT spectroscopy indicate that the same zirconium species is present in the sMAO- $\text{Cp}_2\text{ZrCl}_2$  system. We propose that complex activation results in a surface-supported  $[\text{Cp}^{\text{R}}_2\text{ZrMe}]^+$  species, which is common to all catalysts with the same type of ancillary cyclopentadienyl ligands. Different  $\text{Cp}^{\text{R}}$  ligand sets can result in over an order of magnitude difference in catalyst activity, and can produce different polymer properties.

By variation of the  $\sigma$ -donor (X) groups for simple sMAO- $\text{Cp}_2\text{ZrX}_2$  catalysts we observe smaller, but significant differences in polymerisation activity (ranging from 516 to 1160  $\text{kg}_{\text{PE}} \text{mol}_{\text{Zr}}^{-1} \text{h}^{-1}$ ), which is highest for the sMAO- $\text{Cp}_2\text{Zr}(\text{C}_6\text{F}_5)_2$  system.  $^{19}\text{F}$  NMR spectroscopy data for sMAO- $\text{Cp}_2\text{Zr}(\text{C}_6\text{F}_5)_2$  are consistent with  $\text{C}_6\text{F}_5$  group transfer from Zr to Al during complex activation. Immobilisation of  $\text{Cp}_2\text{ZrMe}_2$  on a  $\text{C}_6\text{F}_5$  modified sMAO support, yields a catalyst system with very similar spectroscopic and polymerisation properties to those of sMAO- $\text{Cp}_2\text{Zr}(\text{C}_6\text{F}_5)_2$ . This provides supporting evidence for a secondary interaction between the  $[\text{Cp}_2\text{ZrMe}]^+$  species and the sMAO surface, which can influence catalytic activity. Further studies are needed to understand the nature of the interactions between the activator surface and the methylzirconocene species, to enable optimisation of both the solid support and complex in catalyst design.

## Conflicts of interest

There are no conflicts to declare.

## Acknowledgements

A. F. R. K., Z. R. T. (SCG Research Fellowship) and J.-C. B. thank SCG Chemicals Co., Ltd (Thailand) for funding. We are grateful to Dr J. V. Lamb (University of Oxford) for SEM imaging, Miss M. George for DSC measurements and Mrs J. A. Holter (David Cockayne Centre for Electron Microscopy, Oxford Materials) for SEM-EDX analysis. We thank the UK 850 MHz solid-state NMR Facility at the University of Warwick for spectrometer time and Dr Dinu Luga for assistance with the 850 MHz ssNMR measurements. We thank Dr S. Sripothongnak for assistance with polymerisation testing. A. F. R. K. also thanks Wadham College Oxford for a R. J. P. Williams Junior Research Fellowship.

## Notes and references

- H. S. Zijlstra and S. Harder, Methylalumoxane—History, Production, Properties, and Applications, *Eur. J. Inorg. Chem.*, 2014, 19–43.
- W. Kaminsky, Discovery of Methylaluminoxane as Cocatalyst for Olefin Polymerization, *Macromolecules*, 2012, **45**, 3289–3297.
- Tailor-Made Polymers*, ed. J. R. Severn and J. C. Chadwick, Wiley-VCH Verlag GmbH & Co. KGaA, Weinheim, Germany, 2008.
- J. R. Severn, J. C. Chadwick, R. Duchateau and N. Friederichs, 'Bound but Not Gagged' Immobilizing Single-Site  $\alpha$ -Olefin Polymerization Catalysts, *Chem. Rev.*, 2005, **105**, 4073–4147.
- C. Janiak, B. Rieger, R. Voelkel and H.-G. Braun, Polymeric aluminosilicates: A possible cocatalytic support material for Ziegler–Natta-type metallocene catalysts, *J. Polym. Sci., Part A: Polym. Chem.*, 1993, **31**, 2959–2968.
- J. Jin, T. Uozumi and K. Soga, Polymerization of olefins with zirconocene catalysts using methylaluminoxane modified with hydroquinone as cocatalyst, *Macromol. Chem. Phys.*, 1996, **197**, 849–854.
- J. Wang, J. Chen and Y. Yang, Micronization of titanocene dichloride by rapid expansion of supercritical solution and its ethylene polymerization, *J. Supercrit. Fluids*, 2005, **33**, 159–172.
- M. Bartke, M. Oksman, M. Mustonen and P. Denifl, A New Heterogenization Technique for Single-Site Polymerization Catalysts, *Macromol. Mater. Eng.*, 2005, **290**, 250–255.
- J. C. Hicks, B. A. Mullis and C. W. Jones, Sulfonic Acid Functionalized SBA-15 Silica as a Methylaluminoxane-Free Cocatalyst/Support for Ethylene Polymerization, *J. Am. Chem. Soc.*, 2007, **129**, 8426–8427.
- E. Kaji and E. Yoshioka, *US Pat.*, 8404880 B2, 8404880 B2, 2013.
- A. F. R. Kilpatrick, J.-C. Buffet, P. Nørby, N. H. Rees, N. P. Funnell, S. Sripothongnak and D. O'Hare, Synthesis and Characterization of Solid Polymethylaluminoxane: A Bifunctional Activator and Support for Slurry-Phase Ethylene Polymerization, *Chem. Mater.*, 2016, **28**, 7444–7450.
- T. J. Williams, J.-C. Buffet, Z. R. Turner and D. O'Hare, Group 4 permethylindenyl constrained geometry complexes for ethylene polymerisation catalysis, *Catal. Sci. Technol.*, 2018, **8**, 5454–5461.
- J.-C. Buffet, Z. R. Turner and D. O'Hare, Popcorn-shaped polyethylene synthesised using highly active supported permethylindenyl metallocene catalyst systems, *Chem. Commun.*, 2018, **54**, 10970–10973.
- J. V. Lamb, J.-C. Buffet, Z. R. Turner and D. O'Hare, Group 4 permethylindenyl complexes for slurry phase polymerisation of ethylene, *Polym. Chem.*, 2019, **10**, 1386–1398.
- T. A. Q. Arnold, Z. R. Turner, J.-C. Buffet and D. O'Hare, Polymethylaluminoxane supported zirconocene catalysts for polymerisation of ethylene, *J. Organomet. Chem.*, 2016, **822**, 85–90.
- J.-C. Buffet, T. A. Q. Arnold, Z. R. Turner, P. Angpanitcharoen and D. O'Hare, Synthesis and characterisation of permethylindenyl zirconium complexes and their use in ethylene polymerisation, *RSC Adv.*, 2015, **5**, 87456–87464.
- A. F. R. Kilpatrick, N. H. Rees, S. Sripothongnak, J.-C. Buffet and D. O'Hare, Slurry-Phase Ethylene Polymerization Using Pentafluorophenyl- and Pentafluorophenoxy-Modified Solid Polymethylaluminoxanes, *Organometallics*, 2018, **37**, 156–164.



- 18 J. V. Lamb, J.-C. Buffet, Z. R. Turner and D. O'Hare, Ethylene Polymerization Using Zirconocenes Supported on Pentafluorophenyl-Modified Solid Polymethylaluminoxane, *Macromolecules*, 2020, **53**, 929–935.
- 19 M. Linnolahti, J. R. Severn and T. A. Pakkanen, Formation of Nanotubular Methylaluminoxanes and the Nature of the Active Species in Single-Site  $\alpha$ -Olefin Polymerization Catalysis, *Angew. Chem., Int. Ed.*, 2008, **47**, 9279–9283.
- 20 Z. Falls, N. Tymińska and E. Zurek, The Dynamic Equilibrium Between (AlOMe)<sub>n</sub> Cages and (AlOMe)<sub>n</sub>·(AlMe<sub>3</sub>)<sub>m</sub> Nanotubes in Methylaluminoxane (MAO): A First-Principles Investigation, *Macromolecules*, 2014, **47**, 8556–8569.
- 21 E. Talsi, The metallocene/methylaluminoxane catalysts formation: EPR spin probe study of Lewis acidic sites of methylaluminoxane, *J. Mol. Catal. A: Chem.*, 1999, **139**, 131–137.
- 22 L. Luo, S. A. Sangokoya, X. Wu, S. P. Diefenbach and B. Kneale, *US Pat.*, 0062492 A1, 2009.
- 23 F. Ghiotto, C. Pateraki, J. Tanskanen, J. R. Severn, N. Luehmann, A. Kusmin, J. Stellbrink, M. Linnolahti and M. Bochmann, Probing the Structure of Methylaluminoxane (MAO) by a Combined Chemical, Spectroscopic, Neutron Scattering, and Computational Approach, *Organometallics*, 2013, **32**, 3354–3362.
- 24 M. A. Henderson, T. K. Trefz, S. Collins, M. Y. Wang and J. S. McIndoe, Characterization of Isobutylaluminoxanes by Electrospray Ionization Mass Spectrometry, *Organometallics*, 2013, **32**, 2079–2083.
- 25 T. K. Trefz, M. A. Henderson, M. Y. Wang, S. Collins and J. S. McIndoe, Mass Spectrometric Characterization of Methylaluminoxane, *Organometallics*, 2013, **32**, 3149–3152.
- 26 J. T. Hirvi, M. Bochmann, J. R. Severn and M. Linnolahti, Formation of octameric methylaluminoxanes by hydrolysis of trimethylaluminum and the mechanisms of catalyst activation in single-site  $\alpha$ -olefin polymerization catalysis, *ChemPhysChem*, 2014, **15**, 2732–2742.
- 27 T. K. Trefz, M. A. Henderson, M. Linnolahti, S. Collins and J. S. McIndoe, Mass Spectrometric Characterization of Methylaluminoxane-Activated Metallocene Complexes, *Chem. – Eur. J.*, 2015, **21**, 2980–2991.
- 28 M. S. Kuklin, J. T. Hirvi, M. Bochmann and M. Linnolahti, Toward Controlling the Metallocene/Methylaluminoxane-Catalyzed Olefin Polymerization Process by a Computational Approach, *Organometallics*, 2015, **34**, 3586–3597.
- 29 H. S. Zijlstra, M. Linnolahti, S. Collins and J. S. McIndoe, Additive and Aging Effects on Methylaluminoxane Oligomers, *Organometallics*, 2017, **36**, 1803–1809.
- 30 H. S. Zijlstra, A. Joshi, M. Linnolahti, S. Collins and J. S. McIndoe, Modifying methylaluminoxane via alkyl exchange, *Dalton Trans.*, 2018, **47**, 17291–17298.
- 31 F. Zaccaria, P. H. M. Budzelaar, R. Cipullo, C. Zuccaccia, A. Macchioni, V. Busico and C. Ehm, Reactivity Trends of Lewis Acidic Sites in Methylaluminoxane and Some of Its Modifications, *Inorg. Chem.*, 2020, **59**, 5751–5759.
- 32 M. E. Z. Velthoen, A. Muñoz-Murillo, A. Bouhmadi, M. Cecius, S. Diefenbach and B. M. Weckhuysen, The Multifaceted Role of Methylaluminoxane in Metallocene-Based Olefin Polymerization Catalysis, *Macromolecules*, 2018, **51**, 343–355.
- 33 M. E. Z. Velthoen, J. M. Boereboom, R. E. Buló and B. M. Weckhuysen, Insights into the activation of silica-supported metallocene olefin polymerization catalysts by methylaluminoxane, *Catal. Today*, 2019, **334**, 223–230.
- 34 M. Atiqullah, M. N. Akhtar, M. Faiz, A. Moman, A. H. Abu Raqabah, J. H. Khan and M. I. Wazeer, Surface chemistry of selected supported metallocene catalysts studied by DR-FTIR, CPMAS NMR, and XPS techniques, *Surf. Interface Anal.*, 2006, **38**, 1319–1327.
- 35 M. Jezequel, V. Dufaud, M. J. Ruiz-Garcia, F. Carrillo-Hermosilla, U. Neugebauer, G. P. Niccolai, F. Lefebvre, F. Bayard, J. Corker, S. Fiddy, J. Evans, J.-P. Broyer, J. Malinge and J.-M. Basset, Supported Metallocene Catalysts by Surface Organometallic Chemistry. Synthesis, Characterization, and Reactivity in Ethylene Polymerization of Oxide-Supported Mono- and Biscyclopentadienyl Zirconium Alkyl Complexes: Establishment of Structure/Reactivity Relationships, *J. Am. Chem. Soc.*, 2001, **123**, 3520–3540.
- 36 D. E. Babushkin, N. V. Semikolenova, V. A. Zakharov and E. P. Talsi, Mechanism of dimethylzirconocene activation with methylaluminoxane: NMR monitoring of intermediates at high Al/Zr ratios, *Macromol. Chem. Phys.*, 2000, **201**, 558–567.
- 37 K. P. Bryliakov, E. P. Talsi and M. Bochmann, <sup>1</sup>H and <sup>13</sup>C NMR Spectroscopic Study of Titanium(IV) Species Formed by Activation of Cp<sub>2</sub>TiCl<sub>2</sub> and [(Me<sub>4</sub>C5)SiMe<sub>2</sub>NtBu]TiCl<sub>2</sub> with Methylaluminoxane (MAO), *Organometallics*, 2004, **2**, 149–152.
- 38 M. E. Z. Velthoen, H. Meeldijk, F. Meirer and B. M. Weckhuysen, Intra- and Interparticle Heterogeneities in Solid Activators for Single-Site Olefin Polymerization Catalysis as Revealed by Micro-Spectroscopy, *Chem. – Eur. J.*, 2018, **24**, 11944–11953.
- 39 F. Blanc, C. Copéret, A. Lesage and L. Emsley, High resolution solid state NMR spectroscopy in surface organometallic chemistry: access to molecular understanding of active sites of well-defined heterogeneous catalysts, *Chem. Soc. Rev.*, 2008, **37**, 518–526.
- 40 L. Reven, Solid-state NMR studies of supported organometallics, *J. Mol. Catal.*, 1994, **86**, 447–477.
- 41 C. Copéret, W.-C. Liao, C. P. Gordon and T.-C. Ong, Active Sites in Supported Single-Site Catalysts: An NMR Perspective, *J. Am. Chem. Soc.*, 2017, **139**, 10588–10596.
- 42 C. Sishta, R. M. Hathorn and T. J. Marks, Group 4 metallocene-aluminoxane olefin polymerization catalysts. CPMAS-NMR spectroscopic observation of cation-like zirconocene alkyls, *J. Am. Chem. Soc.*, 1992, **114**, 1112–1114.
- 43 K. H. Dahmen, D. Hedden, R. L. Burwell and T. J. Marks, Organometallic molecule-support interactions. Highly active organozirconium hydrogenation catalysts and the formation of cationic species on alumina surfaces, *Langmuir*, 1988, **4**, 1212–1214.
- 44 D. G. Cory and W. M. Ritchey, Suppression of signals from the probe in bloch decay spectra, *J. Magn. Reson.*, 1988, **80**, 128–132.



- 45 I. Hung and R. W. Schurko, Solid-State  $^{91}\text{Zr}$  NMR of Bis (cyclopentadienyl) dichlorozirconium(IV), *J. Phys. Chem. B*, 2004, **108**, 9060–9069.
- 46 A. J. Rossini, I. Hung, S. A. Johnson, C. Slebodnick, M. Mensch, P. A. Deck and R. W. Schurko, Solid-State  $^{91}\text{Zr}$  NMR Spectroscopy Studies of Zirconocene Olefin Polymerization Catalyst Precursors, *J. Am. Chem. Soc.*, 2010, **132**, 18301–18317.
- 47 F. H. Larsen, H. J. Jakobsen, P. D. Ellis and N. C. Nielsen, QCPMG-MAS NMR of half-integer quadrupolar nuclei, *J. Magn. Reson.*, 1998, **131**, 144–147.
- 48 R. Siegel, T. T. Nakashima and R. E. Wasylshen, Signal-to-noise enhancement of NMR spectra of solids using multiple-pulse spin-echo experiments, *Concepts Magn. Reson., Part A*, 2005, **26A**, 62–77.
- 49 R. Lefort, J. W. Wiench, M. Pruski and J. P. Amoureux, Optimization of data acquisition and processing in Carr–Purcell–Meiboom–Gill multiple quantum magic angle spinning nuclear magnetic resonance, *J. Chem. Phys.*, 2002, **116**, 2493–2501.
- 50 J. L. Eilertsen, J. A. Støvneng, M. Ystenes and E. Rytter, Activation of metallocenes for olefin polymerization as monitored by IR spectroscopy, *Inorg. Chem.*, 2005, **44**, 4843–4851.
- 51 S. Collins, M. Linnolahti, M. G. Zamora, H. S. Zijlstra, M. T. Rodríguez Hernández and O. Perez-Camacho, Activation of  $\text{Cp}_2\text{ZrX}_2$  (X = Me, Cl) by Methylaluminoxane As Studied by Electrospray Ionization Mass Spectrometry: Relationship to Polymerization Catalysis, *Macromolecules*, 2017, **50**, 8871–8884.
- 52 J. E. O’Gara, K. B. Wagener and S. F. Hahn, Acyclic diene metathesis (ADMET) polymerization. Synthesis of perfectly linear polyethylene, *Makromol. Chem., Rapid Commun.*, 1993, **14**, 657–662.
- 53 G. Rojas, B. Inci, Y. Wei and K. B. Wagener, Precision Polyethylene: Changes in Morphology as a Function of Alkyl Branch Size, *J. Am. Chem. Soc.*, 2009, **131**, 17376–17386.

